A New Fourth-Order Non-Oscillatory Central Scheme For Hyperbolic Conservation Laws

A. A. I. Peer [a,1], A. Gopaul [a], M. Z. Dauhoo [a], M. Bhuruth [a,*]

[a] *Department of Mathematics, University of Mauritius, Reduit, Mauritius*

Abstract

We propose a new fourth-order non-oscillatory central scheme for computing approximate solutions of hyperbolic conservation laws. A piecewise cubic polynomial is used for the spatial reconstruction and for the numerical derivatives we choose genuinely fourth-order accurate non-oscillatory approximations. The solution is advanced in time using natural continuous extension of Runge-Kutta methods. Numerical tests on both scalar and gas dynamics problems confirm that the new scheme is non-oscillatory and sharper than existing fourth-order central schemes when solving profiles with discontinuities. Experiments on nonlinear Burgers' equation indicate that our scheme is superior to existing fourth-order central schemes in the sense that the total variation of the computed solutions are closer to the total variation of the exact solution.

Key words: Hyperbolic Conservation Laws, Central Difference Scheme, Non-Oscillatory Scheme, Total Variation
1991 MSC: 65M10, 65M05

1 Introduction

A variety of high-resolution Godunov-type methods for computing approximate solutions of hyperbolic conservation laws have been proposed by various researchers. Godunov-type schemes are based on the reconstruction of a piecewise-polynomial approximation from cell-averages which is then evolved to the next time level. The

* Author for correspondance.
Email addresses: arshad.peer@umail.uom.ac.mu (A. A. I. Peer), a.gopaul@uom.ac.mu (A. Gopaul), m.dauhoo@uom.ac.mu (M. Z. Dauhoo), mbhuruth@uom.ac.mu (M. Bhuruth).

[1] The research of A. A. I. Peer was supported by a postgraduate research scholarship from the Tertiary Education Commission and the University of Mauritius.

schemes derived in [3,17,6] are of upwind type and those presented in [19,18] are central schemes. The time evolution process in upwind schemes requires the computation of approximate fluxes at cell boundaries and therefore involve solutions of Riemann problems at the discontinuous interfaces.

In recent years, central schemes have gained popularity due to their simplicity as they do not require specific knowledge of the eigenstructure of a given problem and do not involve any Riemann solvers. A second-order central scheme was proposed by Nessyahu and Tadmor [19]. This scheme widely known as the NT scheme is based on the first-order Lax-Friedrichs scheme [2] and involves the reconstruction of piecewise-linear MUSCL-type interpolants from piecewise constant data and uses nonlinear limiters to prevent oscillations. Modifications to the NT scheme with a smaller amount of numerical viscosity were proposed by Kurganov and Tadmor [8]. These modifications are second-order central schemes having a semi-discrete formulation and are based on integration over Riemann fans of variable sizes and make use of more precise information about the local speeds of propagation. Extensions to multidimensional problems can be found in [7].

Generalization of the schemes from [8] were proposed by Kurganov, Noelle and Petrova [9] and these schemes have an upwind nature since they use one-sided local speeds of propagation. The use of one-sided information to estimate the width of the Riemann fans makes these central-upwind schemes less dissipative. Third-order central schemes based on the non-oscillatory third-order reconstruction of Liu and Osher [16] and on staggered evolution of the reconstructed cell averages was proposed by Liu and Tadmor [18]. They showed that this third-order extension is non-oscillatory in the sense that it does not increase the number of initial extrema.

High-order essentially non-oscillatory (ENO) [3] and weighted ENO (WENO) [17,6] reconstructions derived in the upwind framework were first combined with central schemes by Bianco, Puppo and Russo [1]. The time integrals in the third and fourth order central schemes proposed by these authors are evaluated using a quadrature formula and the approximate fluxes at intermediate time steps computed using natural continuous extension of Runge-Kutta method. An improved version of the fourth order scheme of Bianco, Puppo and Russo was presented in [11]. Here a new central weighted nonoscillatory (CWENO) reconstruction for one-dimensional problems was introduced. Other central schemes with WENO polynomials are presented in [12,21] and extensions to multi-dimensional problems can be found in [14,15].

In this paper we propose a new fourth-order central scheme for hyperbolic conservation laws. Following the NT scheme, we derive a scheme which employs a non-oscillatory reconstruction by combining a higher-order polynomial with a mechanism to eliminate oscillations. A numerical study of the behaviour of the total variation is carried out as in [13] and we compare the results for nonlinear scalar waves. It is shown that the total variation for our scheme is closer to that of

the exact solution than for the CWENO scheme in case of the nonlinear Burgers' equation.

This paper is organized as follows. In §2 we give a brief review of Godunov-type central schemes for one-dimensional hyperbolic conservation laws and in §3 we describe the reconstruction steps of the new fourth-order non-oscillatory central method. A linear stability analysis of the new central scheme is carried out in §4 and in §5 we describe the numerical results computed using the newly developed scheme. We show the non-oscillatory behaviour of the new scheme on scalar equations along with the total variation for nonlinear Burgers' equation. Finally we test our scheme on the Euler equations of gas dynamics including complex problems with important shocks.

2 Central Schemes

We are interested in computing approximate solutions to the hyperbolic conservation law

$$u_t + f(u)_x = 0, \quad u \in \mathbb{R}^d,\ d \geq 1, \tag{1}$$

subject to the initial conditions, $u(x,\, t=0) = u_0(x)$.

Consider a uniform spatial grid where the cell $I_j = \left[x_{j-\frac{1}{2}},\, x_{j+\frac{1}{2}}\right]$ has a width h and let $x_j = \left(x_{j-\frac{1}{2}} + x_{j+\frac{1}{2}}\right)/2$ be the mid-cell grid point of I_j. Also let $\Delta t = t^{n+1} - t^n$ and denote by $u_j^n := u(x_j,\, t^n)$. Let the approximation to the cell averages of u on I_j and $I_{j+\frac{1}{2}}$ be given by

$$\bar{u}_j^n = \frac{1}{h}\int_{I_j} u\,(x, t^n)\ dx, \quad \bar{u}_{j+\frac{1}{2}}^n = \frac{1}{h}\int_{I_{j+\frac{1}{2}}} u\,(x, t^n)\ dx.$$

Assuming that the cell averages $\left\{\bar{u}_j^n\right\}$ are known, we look for the cell averages at the next time step t^{n+1}. Let $\chi_j(x)$ be the characteristic function of the cell I_j and let $R_j^n(x)$ be a cubic polynomial in I_j reconstructed from cell averages $\left\{\bar{u}_j^n\right\}$. Define P_u to be the piecewise cubic polynomial given by

$$P_u\,(x,\, t^n) = \sum_j R_j^n(x)\,\chi_j(x). \tag{2}$$

Integrating (1) over $I_{j+\frac{1}{2}} \times [t^n,\, t^{n+1}]$, and using a quadrature formula for the time

integral with (2), we get

$$\bar{u}_{j+\frac{1}{2}}^{n+1} = \frac{1}{h}\int_{x_j}^{x_{j+1}} P_u\left(x,\, t^n\right)\, dx + \lambda \sum_{l=0}^{m} \gamma_l \left[f\left(u(x_j,\, t^n + \beta_l \Delta t)\right) - f\left(u(x_{j+1},\, t^n + \beta_l \Delta t)\right)\right], \qquad (3)$$

where $\lambda = \Delta t/h$, γ_l and β_l are the weights and nodes of the quadrature formula, and $u(x_j,\, t^n + \beta_l \Delta t)$ are the intermediate values. For our numerical tests, we use the Simpson's rule with $\beta_0 = 0$, $\beta_1 = 1/2$, $\beta_2 = 1$, $\gamma_0 = 1/6$, $\gamma_1 = 2/3$ and $\gamma_2 = 1/6$.

The staggered cell averages $\bar{u}_{j+\frac{1}{2}}^{n}$ at time t^n are given by

$$\bar{u}_{j+\frac{1}{2}}^{n} = \frac{1}{h}\int_{x_j}^{x_{j+1}} P_u\left(x,\, t^n\right)\, dx = \frac{1}{h}\left[\int_{x_j}^{x_{j+\frac{1}{2}}} R_j^n(x)\, dx + \int_{x_{j+\frac{1}{2}}}^{x_{j+1}} R_{j+1}^n(x)\, dx\right]. \qquad (4)$$

In the next section, we show how to compute the staggered cell average (4) and the flux of the quadrature formula in (3).

3 A Fourth-Order Non-Oscillatory Reconstruction

In this section we describe the new reconstruction. We choose the interpolating polynomial $R_j^n(x)$ on I_j to have the form

$$R_j^n(x) = u_j^n + u_j'\left(\frac{x - x_j}{h}\right) + \frac{1}{2!}u_j''\left(\frac{x - x_j}{h}\right)^2 + \frac{1}{3!}u_j'''\left(\frac{x - x_j}{h}\right)^3, \quad x \in I_j, \qquad (5)$$

where $R_j^n(x)$ obeys the conservation property $\frac{1}{h}\int_{I_j} R_j^n(x)\, dx = \bar{u}_j^n$, that is, u_j^n must satisfy

$$u_j^n = \bar{u}_j^n - \frac{1}{24}u_j''. \qquad (6)$$

Using (5) and (6), the reconstruction of (4) gives

$$\bar{u}_{j+\frac{1}{2}}^{n} = \frac{1}{2}(\bar{u}_j^n + \bar{u}_{j+1}^n) - \frac{1}{8}(u_{j+1}' - u_j') - \frac{1}{384}(u_{j+1}''' - u_j'''). \qquad (7)$$

We require the numerical derivatives $\frac{1}{h}u'_j$, $\frac{1}{h^2}u''_j$ and $\frac{1}{h^3}u'''_j$ to be fully non-oscillatory compared to ENO reconstructions [11]. The derivatives must also satisfy

$$\frac{1}{h}u'_j = \frac{\partial}{\partial x}u(x = x_j,\, t^n) + \mathcal{O}(h^3), \tag{8}$$

$$\frac{1}{h^2}u''_j = \frac{\partial^2}{\partial x^2}u(x = x_j,\, t^n) + \mathcal{O}(h^2), \tag{9}$$

$$\frac{1}{h^3}u'''_j = \frac{\partial^3}{\partial x^3}u(x = x_j,\, t^n) + \mathcal{O}(h), \tag{10}$$

such that they are genuinely fourth-order accurate.

The NT scheme uses a second-order accurate limiter

$$v'_j = \text{MM}\left(\Delta v_{j-\frac{1}{2}}, \Delta v_{j+\frac{1}{2}}\right), \tag{11}$$

which is non-oscillatory in the sense that

$$0 \le v'_j \cdot sgn(\Delta v_{j\pm\frac{1}{2}}) \le Const. \cdot \left|\text{MM}\left(\Delta v_{j-\frac{1}{2}}, \Delta v_{j+\frac{1}{2}}\right)\right|.$$

Here, $\Delta v_{j+\frac{1}{2}} = v_{j+1} - v_j$, and the MinMod limiter (MM) is defined by

$$\text{MM}(x_1,\, x_2, \ldots) = \begin{cases} \min_p \{x_p\} & \text{if } x_p > 0\ \forall p, \\ \max_p \{x_p\} & \text{if } x_p < 0\ \forall p, \\ 0 & \text{otherwise.} \end{cases}$$

However, the accuracy of (11) drops at the non-sonic critical gridvalues v_j, where $\Delta v_{j-\frac{1}{2}} \cdot \Delta v_{j+\frac{1}{2}} < 0 \neq f'(v_j)$. NT scheme adapted the uniform non-oscillatory (UNO) limiter of Harten and Osher [4]

$$v'_j = \text{MM}\left(\Delta v_{j-\frac{1}{2}} + \frac{1}{2}\text{MM}\left(\Delta^2 v_{j-1},\, \Delta^2 v_j\right),\, \Delta v_{j+\frac{1}{2}} - \frac{1}{2}\text{MM}\left(\Delta^2 v_j,\, \Delta^2 v_{j+1}\right)\right), \tag{12}$$

where $\Delta^2 v_j = v_{j+1} - 2v_j + v_{j-1}$. The limiter (12) adds second-order differences to the MinMod limiter (11) to achieve high accuracy including at critical points.

In order to get fourth-order accuracy for (8), (9) and (10) we employ the modified UNO limiter of [20]. Analogous to the numerical derivative (11), u'''_j depends on its two neighbouring third-order differences

$$u'''_j = \text{MM}\left(\Delta^3 \bar{u}_{j-\frac{1}{2}}, \Delta^3 \bar{u}_{j+\frac{1}{2}}\right), \tag{13}$$

where $\Delta^3 \bar{u}_{j+\frac{1}{2}} = \Delta^2 \bar{u}_{j+1} - \Delta^2 \bar{u}_j$. Similar to the UNO limiter, u'_j of [20] combines

higher-order terms in smooth regions to attain a high-order accuracy

$$u'_j = \text{MM}\left(\Delta\bar{u}_{j-\frac{1}{2}} + \frac{1}{2}\text{MM}\left(\Delta^2\bar{u}_{j-1} + \nu_1 u'''_{j-1}, \Delta^2\bar{u}_j + \nu_2 u'''_j\right),\right. \tag{14}$$
$$\left.\Delta\bar{u}_{j+\frac{1}{2}} - \frac{1}{2}\text{MM}\left(\Delta^2\bar{u}_j + \nu_3 u'''_j, \Delta^2\bar{u}_{j+1} + \nu_4 u'''_{j+1}\right)\right).$$

A Taylor-expansion of (14) reveals that choosing $\nu_1 = \frac{7}{12}$, $\nu_2 = -\frac{5}{12}$, $\nu_3 = \frac{5}{12}$, $\nu_4 = -\frac{7}{12}$ gives fourth-order order accurate approximations of the first derivative. As in the UNO algorithm, the reconstruction presented here has a wider stencil with respect to piecewise quadratic WENO. This stencil allows the limiter to avoid discontinuities. However, in case extremas cannot be avoided, the accuracy of the modified non-linear limiters (13) and (14) decreases until non-oscillatory approximations are obtained. This mechanism is aimed at removing spurious oscillations allowed by other reconstructions like ENO and its weighted version.

3.1 The Reconstruction of Point-Values

We approximate the point-value u_j^n of (6) from the cell averages $\{\bar{u}_j^n\}$, while simultaneously looking for high accuracy and avoiding oscillations. This is achieved by letting the second-order term of (6) to be

$$u''_j = \text{MM}\left(\Delta^2\bar{u}^n_{j-1} + u'''_{j-1},\, \Delta^2\bar{u}^n_j,\, \Delta^2\bar{u}^n_{j+1} - u'''_{j+1}\right), \tag{15}$$

where the MM limiter with three arguments can be written in the form

$$\begin{aligned}\text{MM}(x_1,\, x_2,\, x_3) =& \frac{1}{4}(\text{sign}(x_1) + \text{sign}(x_2) + \text{sign}(x_3) + \text{sign}(x_1\, x_2\, x_3))\\ &\times \min(|x_1|, |x_2|, |x_3|).\end{aligned}$$

In order to obtain the flux of the quadrature formula in (3), we need different intermediate time values which may be obtained from ODE solvers or Taylor series expansions [18]. However, for both approaches, we need to restart the whole procedure for each intermediate level. Bianco, Puppo and Russo [1] proposed the use of Natural Continuous Extension (NCE) of Runge-Kutta (RK) schemes [26] in order to increase the computational efficiency.

For the fourth-order RK-NCE scheme there exist four third-order polynomials

$$\begin{aligned}b_1(\theta) &= 2(1-4b_1)\theta^3 + 3(3b_1-1)\theta^2 + \theta,\\ b_i(\theta) &= 4(3c_i-2)b_i\theta^3 + 3(3-4c_i)b_i\theta^2, \quad i = 2,3,4,\end{aligned}$$

where $c_i = \sum_j a_{ij}$ and the coefficients b_i and a_{ij} are given by

$$b = \begin{pmatrix} 1/6 \\ 1/3 \\ 1/3 \\ 1/6 \end{pmatrix}, \quad a = \begin{pmatrix} 0 & 0 & 0 & 0 \\ 1/2 & 0 & 0 & 0 \\ 0 & 1/2 & 0 & 0 \\ 0 & 0 & 1 & 0 \end{pmatrix}. \tag{16}$$

To compute the predicted values of the quadrature formula $u(x_j, t^n + \beta_l \Delta t)$ efficiently, we rewrite the fourth-order RK-NCE method as

$$\begin{aligned} u(x_j,\, t^n + \beta_l \Delta t) &= u_j^n + \lambda \sum_{i=1}^{4} b_i(\beta_l) K_{i,j}, \\ K_{i,j} &= -f'(Y_j^i), \\ Y_j^i &= u_j^n + \lambda \sum_{s=1}^{i-1} a_{is} K_{s,j}, \end{aligned} \tag{17}$$

where the coefficients a_{ij} are given in (16), and the numerical derivative satisfies

$$\frac{1}{h} f'(u_j) = \frac{\partial}{\partial x} f(u(x = x_j,\, t^n)) + \mathcal{O}(h^3).$$

We approximate f'_j in a similar way to (14) by combining high-order differences in smooth regions to obtain the desired order of accuracy and still remain non-oscillatory. The first derivative of the fluxes is given by

$$\begin{aligned} f'_j = \text{MM}\Big(\Delta f_{j-\frac{1}{2}} + \frac{1}{2}\text{MM}\Big(\Delta^2 f_{j-1} + \frac{2}{3} f'''_{j-1}, \Delta^2 f_j - \frac{1}{3} f'''_j\Big), \\ \Delta f_{j+\frac{1}{2}} - \frac{1}{2}\text{MM}\Big(\Delta^2 f_j + \frac{1}{3} f'''_j, \Delta^2 f - \frac{2}{3} f'''_{j+1}\Big)\Big), \end{aligned} \tag{18}$$

where

$$f'''_j = \text{MM}\left(\Delta^3 f_{j-\frac{1}{2}}, \Delta^3 f_{j+\frac{1}{2}}\right).$$

Our scheme is summarized in the following algorithm:
step 1: Compute the numerical derivatives u'_j, u''_j and u'''_j given by (14), (15) and (13).
step 2: Compute the point values u_j^n using (6). Use these results to find the numerical derivative $f'(u_j^n)$ with (18).
step 3: Compute the predicted values $u(x_j,\, t^n + \beta_l \Delta t)$ from the RK scheme (17) with NCE. Compute the first derivative of the flux $f'(Y_j^i)$ with (18), notably for $\beta_1 = 1/2$ and $\beta_2 = 1$ (Simpson's quadrature rule).

step 4: Compute the staggered cell-averages at time t^{n+1} according to (3),

$$\bar{u}_{j+\frac{1}{2}}^{n+1} = \frac{1}{2}(\bar{u}_j^n + \bar{u}_{j+1}^n) - (g_{j+1} - g_j)\,, \tag{19}$$

where the modified numerical flux g_j is obtained by rearranging (7) into (3) and using Simpson's quadrature formula and is given by

$$g_j = \frac{1}{384}\left(48u_j' + u_j'''\right) + \frac{\lambda}{6}\left(f(u_j^n) + 4f(u_j^{n+1/2}) + f(u_j^{n+1})\right). \tag{20}$$

We remark that the scheme can be made non-staggered following [5].

4 Stability Analysis

In this section, we carry out a linear stability analysis, similar to that carried out in [1], of the new central staggered scheme (19) and (20), called CNO4, in order to obtain its critical Courant number by applying it to the linear advection equation

$$u_t + u_x = 0.$$

We assume that on smooth profiles the approximations by the MinMod limiter allow stencils on a maximum of cells, that is, the accuracy does not degenerate. Since the approximations can be done on a variety of stencils, we proceed with an analysis on a fixed stencil. Then we express CNO4 in terms of cell-averages only, which is given by $\bar{u}_j^n = \rho^n \mathrm{e}^{\imath\, j\, \xi}$ where $\imath^2 = -1$. On making the substitutions in CNO4 for linear advection equation, we obtain

$$\bar{u}_{j+\frac{1}{2}}^{n+1} = \rho_\lambda(\xi)\mathrm{e}^{\imath\,\xi/2}\bar{u}_j^n, \quad \xi \in [0,\, 2\pi].$$

Let λ^* be the maximum value of λ for which the amplification factor satisfies

$$\max_{0\le\xi\le 2\pi} |\rho_\lambda(\xi)| \le 1. \tag{21}$$

A scheme is said to be stable if $\lambda^* > 0$. In Table 1 we give the different fixed stencils used and their corresponding stability region obtained from (21).

Table 1
Stability analysis of stencils for CNO4

u_j'''	u_j''	Stencil of u_j' and f_j'	Stability Region
$\Delta^3\bar{u}_{j-\frac{1}{2}}$	$\Delta^2\bar{u}_{j-1} + \Delta^3\bar{u}_{j-\frac{3}{2}}$	$j-3,\, j-2,\, j-1,\, j$	unstable
$\Delta^3\bar{u}_{j-\frac{1}{2}}$	$\Delta^2\bar{u}_j$	$j-2,\, j-1,\, j,\, j+1$	$\lambda^* = 0.3408$
$\Delta^3\bar{u}_{j+\frac{1}{2}}$	$\Delta^2\bar{u}_j$	$j-1,\, j,\, j+1,\, j+2$	$\lambda^* = 0.4350$
$\Delta^3\bar{u}_{j+\frac{1}{2}}$	$\Delta^2\bar{u}_{j+1} - \Delta^3\bar{u}_{j+\frac{3}{2}}$	$j,\, j+1,\, j+2,\, j+3$	unstable

We observe that the far left and far right stencils are unstable, but they are the least to occur in CNO4. We choose the critical Courant number as $\lambda_{\max} = 0.3408$ which satisfies the two central stable stencils. We note that CNO4 allows a larger Courant number than CWENO [11], $\lambda_{\max} = 2/7$, though the latter is computed on a smaller stencil.

5 Numerical Experiments

5.1 Scalar Test Problems

We describe the results of numerical experiments using some scalar test problems with periodic boundary conditions over the domain $[-1,\, 1]$. We test the total variation (TV), where $\text{TV}(u) = \sum_j |u_{j+1} - u_j|$ of the numerical experiments. A scheme is called TV bounded (TVB) if $\text{TV}(u^n) \leq K$ for all n and where K is a fixed positive constant.

Problem 5.1: We begin with the linear advection equation $u_t + u_x = 0$, over the long time interval $T = 10$, with the smooth initial condition $u(x,\, 0) = \sin(\pi x)$. We solve the problem with $\lambda = 0.9\lambda_{\max}$. The L_1 and L_∞ errors and orders of convergence are shown in Table 2. We see the CNO4 converges to fourth accuracy in L_1 as the computational grid is refined. Serna and Marquina [22] reported that non-smooth limiters lack regularity and make the schemes less accurate, that is, they do not achieve the maximum expected order of accuracy. Comparing the magnitude of errors produced by CNO4 and CWENO [11] for this test problem shows that CWENO performs better and attains full fourth-order accuracy when solving problems without discontinuities.

Table 2
Errors and orders of convergence for the linear advection problem 5.1

N	L_1 error	L_1 order	L_∞ error	L_∞ order
40	0.1371(-2)	–	0.1986(-2)	–
80	0.9730(-4)	3.8161	0.2239(-3)	3.1490
160	0.6912(-5)	3.8152	0.2512(-4)	3.1562
320	0.4695(-6)	3.8801	0.2792(-5)	3.1696
640	0.3135(-7)	3.9043	0.3088(-6)	3.1764

Problem 5.2: We consider the linear advection equation $u_t + u_x = 0$, over the time interval $T = 4$, with the initial condition given by the square wave $u(x,\, 0) = 1$ for $|x| < 1/3$ and $u(x,\, 0) = 0$ elsewhere. In Table 3 we give the errors by CNO4 and

CWENO using $\lambda = 0.9\lambda_{\max}$. We note that CNO4 yields better accuracy in L_1 than CWENO, though the errors become almost the same as the grid is refined.

Table 3
Errors for approximation of Problem 5.2 at $T = 4$

	CWENO		CNO4	
N	L_1 error	L_∞ error	L_1 error	L_∞ error
25	0.2060	0.4185	0.1903	0.3870
50	0.1192	0.4072	0.1102	0.4068
100	0.6765(-1)	0.4224	0.6477(-1)	0.4246
200	0.3823(-1)	0.4360	0.3801(-1)	0.4395

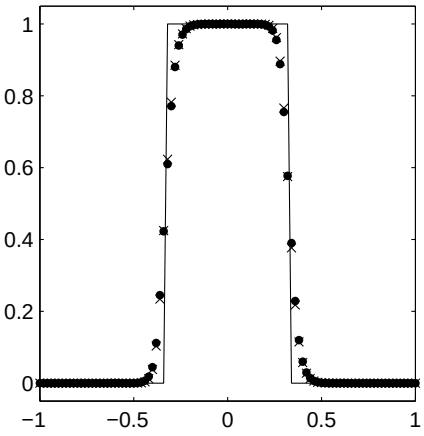

(a)

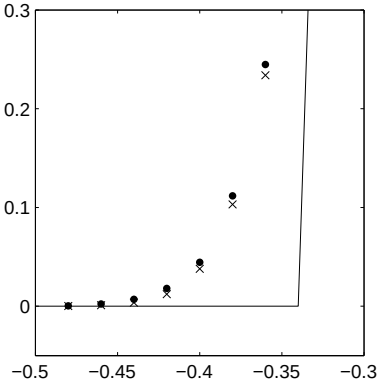

(b) Zoomed region-left foot

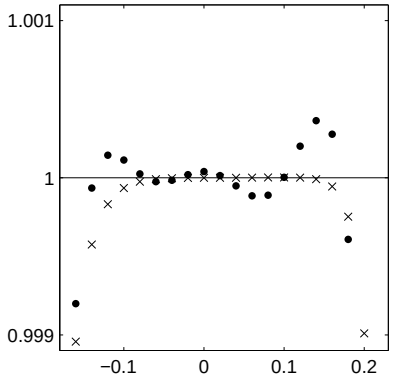

(c) Zoomed region-wave top

Fig. 1. Problem 5.2 by CNO4 "$\times$" and CWENO "$\cdot$" with $N = 100$ at $T = 4$.

In Fig 1 we display the different approximations on 100 cells. We observe that CNO4 gives an overall better approximation than CWENO and is sharper at the foot of the wave. CNO4 is non-oscillatory contrary to CWENO which generates oscillations at top of the wave.

Problem 5.3: Consider the inviscid Burgers' equation $u_t + (0.5\,u^2)_x = 0$, with the initial condition $u(x,\,0) = 1 + 0.5\sin(\pi x)$ and $\lambda = \frac{2}{3}\,\lambda_{\max}$.

Table 4
Errors and orders of convergence for problem 5.3

N	L_1 error	L_1 order	L_∞ error	L_∞ order
Burgers' equation before the shock, $T = 0.12$				
40	0.1928(-4)	–	0.4114(-4)	–
80	0.1193(-5)	4.0153	0.3981(-5)	3.3693
160	0.8135(-7)	3.8738	0.3931(-6)	3.3401
320	0.5398(-8)	3.9137	0.4356(-7)	3.1739
Burgers' equation after the shock, $T = 1.5$				
40	0.6776(-2)	–	0.6023(-1)	–
80	0.3211(-2)	1.0773	0.6179(-1)	-0.0368
160	0.1588(-2)	1.0158	0.6150(-1)	0.0067
320	0.7833(-3)	1.0197	0.6048(-1)	0.0242

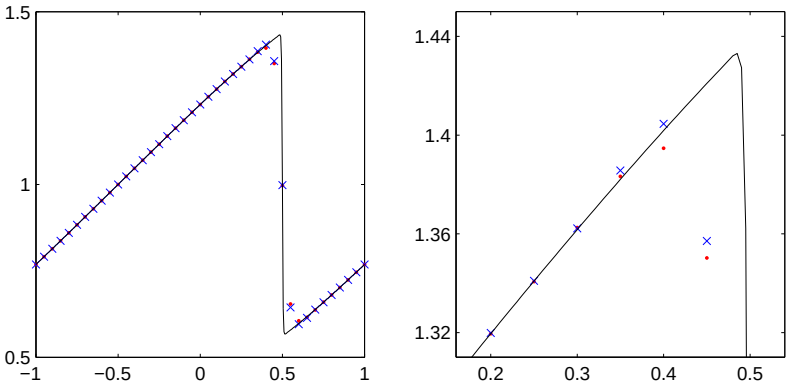

(a) Burger's equation (b) Zoomed region

Fig. 2. Problem 5.3 with $N = 40$ and $T = 1.5$ by CNO4 "$\times$" and CWENO "$\cdot$".

In Table 4, we give the results by CNO4 before and after a shock formation at $T = 0.12$ and $T = 1.5$. Similar to the linear problem 5.1, the L_1 order of convergence

before the shock is nearly 4, whereas the L_∞ order of convergence is nearer to 3. Computing the numerical results (not shown here) reveals that the approximations by CWENO attains full fourth-order convergence at $T = 0.12$. However CNO4 gives errors of smaller magnitude than CWENO after the shock formation.

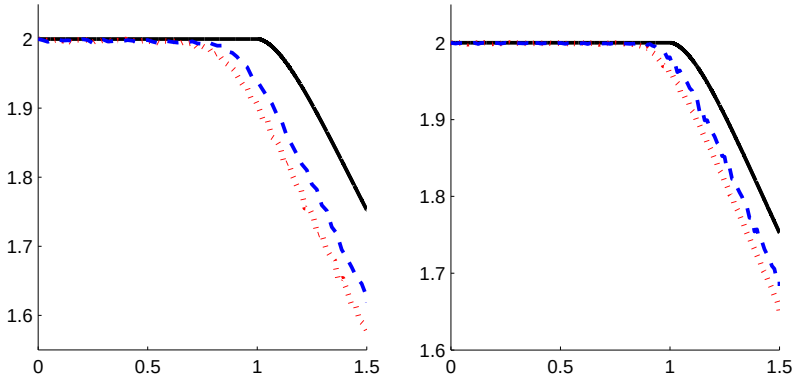

(a) $N = 40$ (b) $N = 80$

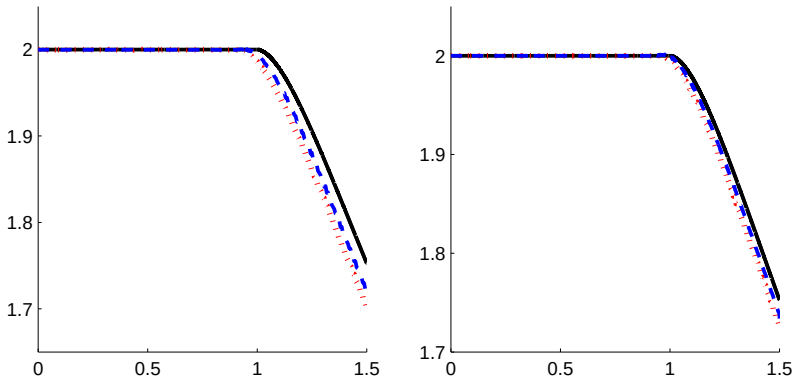

(c) $N = 160$ (d) $N = 320$

Fig. 3. TV of approximations for Problem 5.3 (—: Exact, - -: CNO4, $\cdots$: CWENO).

The approximations at $T = 1.5$ on 40 cells are illustrated in Fig 2. We observe that CNO4 is sharper than CWENO when resolving the shock. In Fig 3, we show the TV at $T = 1.5$ for different number of cells with CNO4 and CWENO. Both numerical results converge to the exact one, but we can see that the computed TV from CNO4 are nearer to the TV of the exact solution.

Problem 5.4: We solve the inviscid Burgers' equation $u_t + (0.5\,u^2)_x = 0$, with the initial condition $u(x,\,0) = 1$ for $|x| < 1/3$ and $u(x,\,0) = 0$ elsewhere. In Fig 4, we show the TV up to time $T = 0.64$, for different number of cells with CNO4 and CWENO with $\lambda = \frac{2}{3}\,\lambda_{\max}$. For this problem, the TV of the exact solution remains 2.

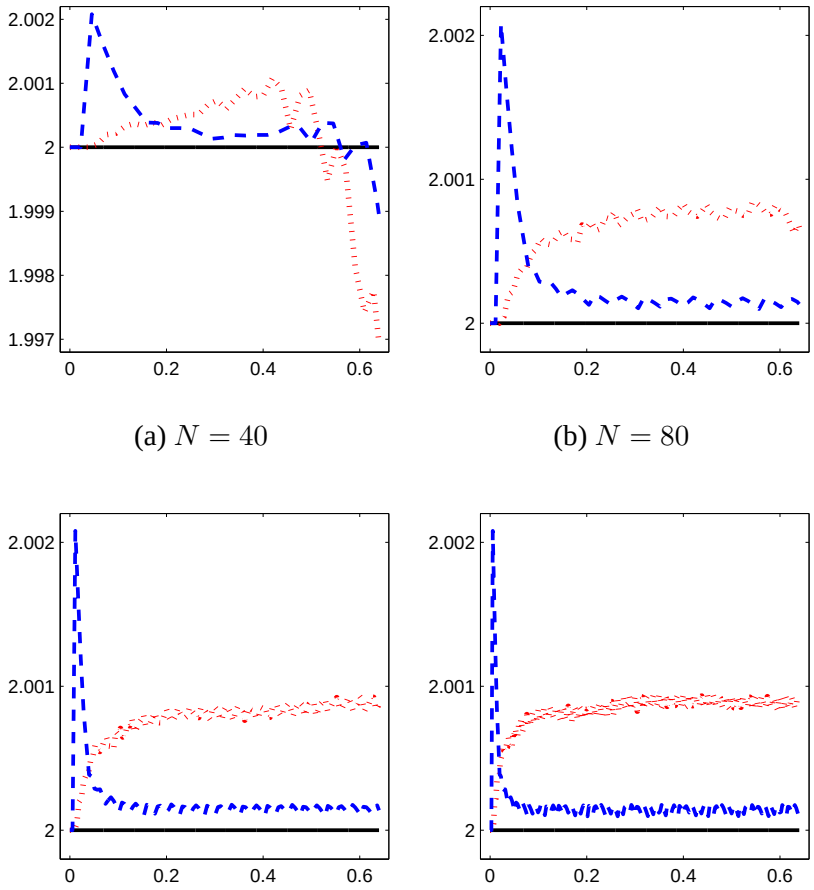

(a) $N = 40$ (b) $N = 80$

(c) $N = 160$ (d) $N = 320$

Fig. 4. TV of approximations for Problem 5.4 (—: Exact, - -: CNO4, $\cdots$: CWENO).

Table 5
Errors for Burger's problem 5.4 at $T = 0.64$

N	CWENO		CNO4	
	L_1 error	L_∞ error	L_1 error	L_∞ error
40	0.6380(-1)	0.5659	0.5857(-1)	0.5608
80	0.2694(-1)	0.3340	0.2407(-1)	0.3273
160	0.1428(-1)	0.4423	0.1267(-1)	0.4399
320	0.6437(-2)	0.3167	0.5983(-2)	0.3217

For $N = 40$, the TV by both CNO4 and CWENO oscillates. For $N = 80, 160$ and 320, we note that CNO4 gives a TV bounded by a maximum in the form of a peak reached after the first few steps and is then damped. The maximum bound is obtained earlier in time as the grid is refined, and then the TV comes close to

the exact one. However, the peak does not seem to depend on the cell width. We also observe that CWENO overestimates the total variations more than CNO4 as the problem is advanced in time.

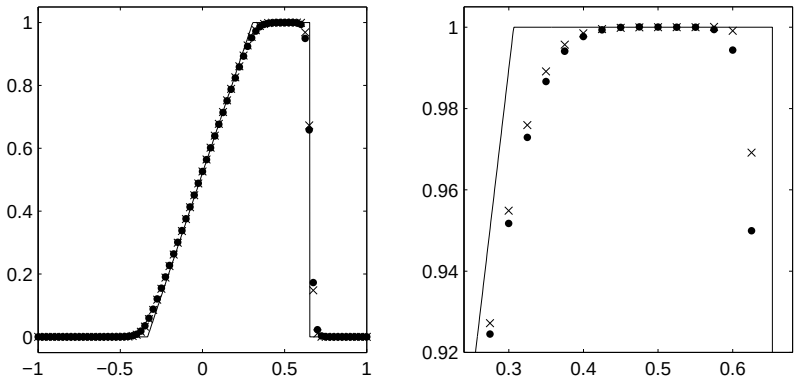

(a) Burger's equation (b) Zoomed region

Fig. 5. Problem 5.4 with $N = 80$ by CNO4 "$\times$" and CWENO "$\cdot$".

In Table 5 we give the corresponding errors for the respective number of cells and we note that CNO4 yields better accuracy than CWENO in L_1. We end this problem with the solution on 80 cells in Fig 5. CNO4 is sharper than CWENO on the expansion wave and the shock.

5.2 Systems of Conservation Laws

We extend our scheme to solve hyperbolic systems of conservation laws

$$U_t + F(U)_x = 0,$$

where the Jacobian $A(U)$ of the flux $F(U)$ has distinct real eigenvalues. We solve the Euler equations of gas dynamics for a polytropic (calorically ideal) gas:

$$\frac{\partial}{\partial t}\begin{bmatrix}\rho\\ \rho q\\ E\end{bmatrix} + \frac{\partial}{\partial x}\begin{bmatrix}\rho q\\ \rho q^2 + p\\ q(E+p)\end{bmatrix} = 0, \quad p = (\gamma-1)(E - \frac{1}{2}\rho q^2). \tag{22}$$

Here ρ, q, p and E are respectively the density, velocity, pressure and total energy of the conserved fluid, and the ratio of the specific heats $\gamma = 1.4$.

There are two methods to extend the numerical schemes considered, namely by doing a componentwise extension or using characteristic decomposition. In the

present work, we adopt the componentwise extension which is less costly. Most central schemes (e.g. [1,11]) fix the CFL number differently for each gas dynamics problem solved. However, this practice requires a knowledge of the problem. Here, we adopt a general strategy to advance in time by using an adaptive evaluation of the time step,

$$\Delta t = \frac{0.9\,\lambda_{\max}\,h}{\max_j(c_j + |q_j|)},$$

where c_j and q_j are the local sound speed and velocity respectively. This time step evaluation technique can accommodate for problems where the characteristic speeds change wildly in time [11].

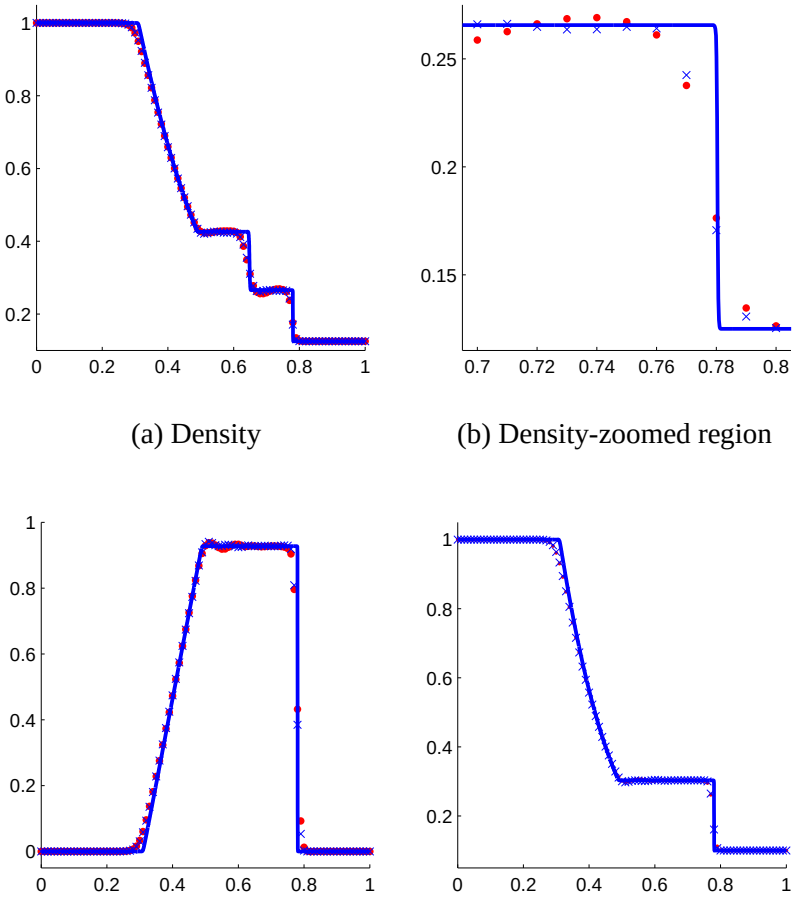

(a) Density (b) Density-zoomed region

(c) Velocity (d) Pressure

Fig. 6. Sod Problem with $N = 100$ by CNO4 “x” and CWENO“.”.

Sod’s Problem [24]: We solve (22) up to $T = 0.16$ with the initial condition

$$U(x,0) = \begin{cases} (1,0,2.5)^T, & 0 \le x < 0.5, \\ (0.125,0,0.25)^T, & 0.5 \le x \le 1. \end{cases}$$

We observe in Fig 6 that CNO4 is sharper and less oscillatory than CWENO in particular for the density profile of this Riemann problem.

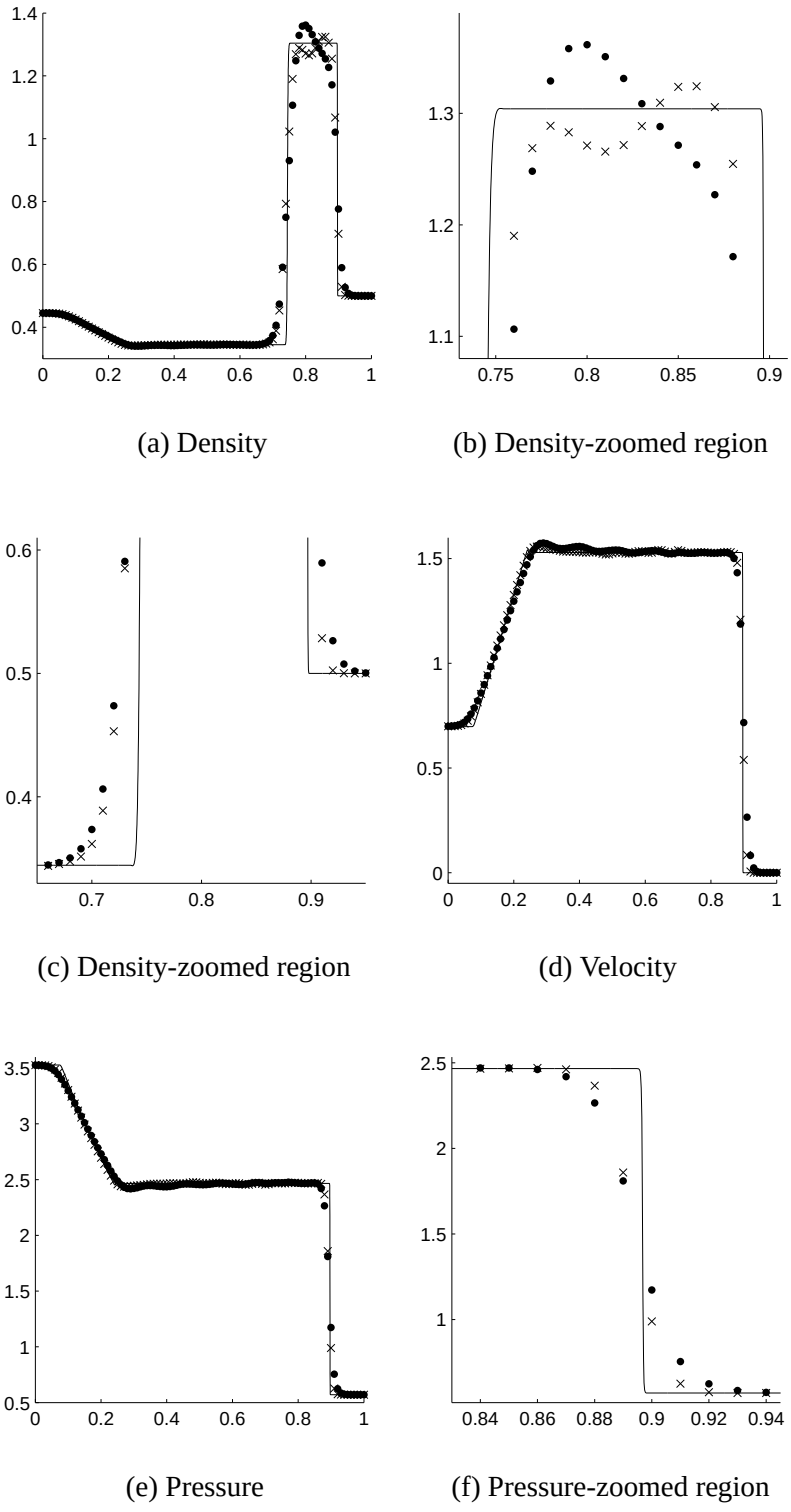

(a) Density (b) Density-zoomed region

(c) Density-zoomed region (d) Velocity

(e) Pressure (f) Pressure-zoomed region

Fig. 7. Lax Problem with $N = 100$ by CNO4 "$\times$" and CWENO "$\cdot$".

Lax's Problem [10]: We solve (22) using the initial condition

$$U(x,0) = \begin{cases} (0.445, 0.31061, 8.92840289)^T, & 0 \le x < 0.5, \\ (0.5, 0, 1.4275)^T, & 0.5 \le x \le 1. \end{cases}$$

For this more severe shock tube problem, the different approximations at time $T = 0.16$ are ilustrated in Fig 7. Similar to the Sod's problem, CNO4 is sharper than CWENO and CWENO generates oscillations near discontinuities. In the density profile shown in Fig 7 (b), CWENO produces overshoots which are decreased in the approximations by CNO4.

Shock-Entropy Test [23]: We consider here a moving Mach 3 shock interacting with sine waves in density.

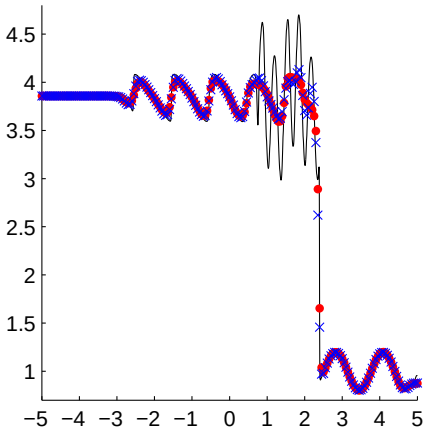

(a) Density

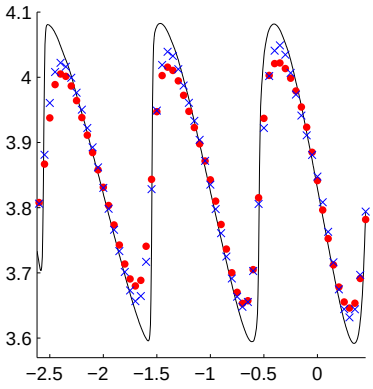

(b) Zoomed region

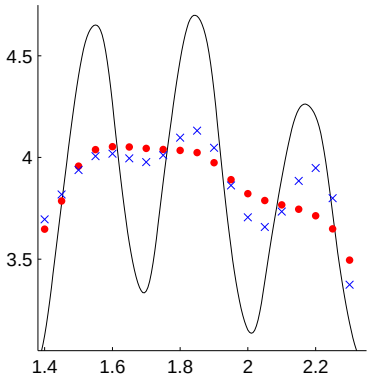

(c) Zoomed region

Fig. 8. Density profile of the Shock-Entropy Test by CNO4 "×" and CWENO "·".

The initial data is given by

$$U(x,0) = \begin{cases} (3.85714,\ 10.1418096304,\ 39.16655928489427)^T,\ -5 \le x < -4, \\ (1 + 0.2\sin(5x),\ 0,\ 2.5)^T, \qquad\qquad -4 \le x \le -5. \end{cases}$$

We test here the performance of the schemes in smooth regions and the ability to capture shocks with relatively spaced cells, $h = 0.05$. We give the numerical approximations of the density profile in Fig. 8 at $T = 1.8$ along with the "exact" solution computed by CWENO with $N = 2000$. We observe in the zoomed regions that CNO4 is sharper than CWENO and that the latter is damped in Fig 8 (c).

Woodward and Colella Bang [25]: Next we consider a shock interaction problem with reflective boundary conditions given by the initial data

$$U(x,0) = \begin{cases} (1, 0, 2500)^T,\ \ 0 \le x < 0.1, \\ (1, 0, 0.025)^T,\ 0.1 \le x < 0.9, \\ (1, 0, 250)^T,\quad 0.9 \le x \le 1. \end{cases}$$

We display the numerical results of the density profile of this complex problem in Fig 9. The results are with $N = 800$ at time $T = 0.038$, and we get the "exact" solution from CWENO on 4000 cells. We observe that CNO4 captures the shocks interaction, and in the zoomed region we see that CNO4 is sharper and behaves better with respect to oscillations compared to CWENO on 800 cells.

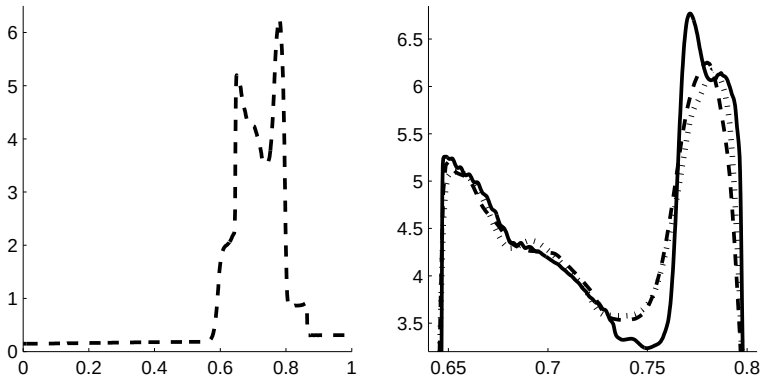

(a) Density (b) Zoomed region

Fig. 9. Density profile of Woodward and Colella Bang with $N = 800$ (—: Exact, - -: CNO4, $\cdots$: CWENO).

6 Conclusion

We have introduced a new fourth-order non-oscillatory central scheme. A piecewise cubic polynomial is used for the reconstruction which uses genuinely fourth-order accurate approximation for the first, second and third order spatial derivatives to avoid spurious oscillations. Numerical experiments on scalar problems show that the scheme resolves discontinuities sharply while maintaining a non-oscillatory profile. In comparison to the CWENO method, the total variation of the numerical solution computed by our scheme for Burger's equation is closer to the total variation of the exact solution. We have also shown that the total variation of the numerical solution by the fourth-order non-oscillatory central scheme is bounded for the test cases considered. The fourth-order non-oscillatory central scheme was then extended to solve hyperbolic systems of conservation laws using an adaptive evaluation of the time step. We observed that for Euler equations of gas dynamics, the proposed scheme is robust and performs better. The new fourth-order scheme is less damped in smooth regions and captures shocks while avoiding oscillations.

References

[1] F. Bianco, G. Puppo, and G. Russo. High-order central schemes for hyperbolic systems of conservation laws. *SIAM J. Sci. Comput.*, 21(1):294–322, 1999.

[2] K. O. Friedrichs and P. D. Lax. Systems of conservation equations with a convex extension. *Proc. Nat. Acad. Sci.*, 68:1686–1688, 1971.

[3] A. Harten, B. Engquist, S. Osher, and S. Chakravarthy. Uniformly high order accurate essentially non-oscillatory schemes, III. *J. Comput. Phys.*, 71:231–303, 1987.

[4] A. Harten and S. Osher. Uniformly high-order accurate nonoscillatory schemes, I. *SIAM J. Numer. Anal.*, 24(2):279–309, 1987.

[5] G. S. Jiang, D. Levy, C. T. Lin, S. Osher, and E. Tadmor. High-resolution nonoscillatory central schemes with nonstaggered grids for hyperbolic conservation laws. *SIAM J. Numer. Anal.*, 35(6):2147–2168, 1998.

[6] G. S. Jiang and C. W. Shu. Efficient implementation of weighted ENO schemes. *J. Comput. Phys.*, 126:202–228, 1996.

[7] G. S. Jiang and E. Tadmor. Nonoscillatory central schemes for multidimensional hyperbolic conservation laws. *SIAM J. Sci. Comput.*, 19(6):1892–1917, 1998.

[8] A. Kurganov and D. Levy. A third-order semidiscrete central scheme for conservation laws and convection-diffusion equations. *SIAM J. Sci. Comput.*, 22(4):1461–1488, 2000.

[9] A. Kurganov, S. Noelle, and G. Petrova. Semidiscrete central-upwind schemes for hyperbolic conservation laws and Hamilton-Jacobi equations. *SIAM J. Sci. Comput.*, 23(3):707–740, 2001.

[10] P. D. Lax. Weak solutions of nonlinear hyperbolic equations and their numerical computation. *Comm. Pure Appl. Math.*, 7:159–193, 1954.

[11] D. Levy, G. Puppo, and G. Russo. Central WENO schemes for hyperbolic systems of conservation laws. *Math. Model. Numer. Anal.*, 33(3):547–571, 1999.

[12] D. Levy, G. Puppo, and G. Russo. Compact central WENO schemes for multidimensional conservation laws. *SIAM J. Sci. Comput.*, 22(2):656–672, 2000.

[13] D. Levy, G. Puppo, and G. Russo. On the behavior of the total variation in CWENO methods for conservation laws. *Appl. Numer. Math.*, 33:407–414, 2000.

[14] D. Levy, G. Puppo, and G. Russo. A third order central WENO scheme for 2D conservation laws. *Appl. Numer. Math.*, 33:415–421, 2000.

[15] D. Levy, G. Puppo, and G. Russo. A fourth-order central WENO scheme for multidimensional hyperbolic systems of conservation laws. *SIAM J. Sci. Comput.*, 24(2):480–456, 2002.

[16] X. D. Liu and S. Osher. Nonoscillatory high order accurate self-similar maximum principle satisfying shock capturing schemes I. *SIAM J. Numer. Anal.*, 33(2):760–779, 1996.

[17] X. D. Liu, S. Osher, and T. Chan. Weighted essentially non-oscillatory schemes. *J. Comput. Phys.*, 115:200–212, 1994.

[18] X. D. Liu and E. Tadmor. Third order nonoscillatory central scheme for hyperbolic conservation laws. *Numer. Math.*, 79:397–425, 1998.

[19] H. Nessyahu and E. Tadmor. Non-oscillatory central differencing for hyperbolic conservation laws. *J. Comput. Phys.*, 87(2):408–463, 1990.

[20] A. A. I. Peer, A. Gopaul, M. Z. Dauhoo, and M. Bhuruth. New high-order ENO reconstructions for hyperbolic conservation laws. In *Proceedings of the 2005 Conference on Computational and Mathematical Methods on Science and Engineering*, pages 446–455, 2005.

[21] J. Qiu and C. W. Shu. On the construction, comparison, and local characteristic decomposition for high-order central WENO schemes. *J. Comput. Phys.*, 183:187–209, 2002.

[22] S. Serna and A. Marquina. Power ENO methods: a fifth-order accurate Weighted Power ENO method. *J. Comput. Phys.*, 194:632–658, 2004.

[23] C. W. Shu and S. Osher. Efficient implementation of essentially non-oscillatory shock-capturing schemes II. *J. Comput. Phys.*, 83:32–78, 1989.

[24] G. Sod. A survey of several finite difference methods for systems of nonlinear hyperbolic conservation laws. *J. Comput. Phys.*, 27:1–31, 1978.

[25] P. Woodward and P. Colella. The numerical simulation of two-dimensional fluid flow with strong shocks. *J. Comput. Phys.*, 54:115–173, 1984.

[26] M. Zennaro. Natural continuous extensions of Runge-Kutta methods. *Math. Comp.*, 46:119–133, 1986.